

# GCF: Generalized Causal Forest for Heterogeneous Treatment Effect Estimation in Online Marketplace

Shu Wan\*  
Chen Zheng\*  
wanshu@didiglobal.com  
zhengchen@didiglobal.com  
Didi Chuxing  
Beijing, China

Zhonggen Sun  
Mengfan Xu  
sun@didiglobal.com  
melodyxumengfan@didiglobal.com  
Didi Chuxing  
Beijing, China

Xiaoqing Yang  
yangxiaoqing@didiglobal.com  
Didi Chuxing  
Beijing, China

Hongtu Zhu  
hongtuzhu@didiglobal.com  
AI Labs, Didi Chuxing  
Beijing, China

Jiecheng Guo  
jasonguo@didiglobal.com  
Didi Chuxing  
Beijing, China

## ABSTRACT

Uplift modeling is a rapidly growing approach that utilizes machine learning and causal inference methods to estimate the heterogeneous treatment effects. It has been widely adopted and applied to online marketplaces to assist large-scale decision-making in recent years. The existing popular methods, like forest-based modeling, either work only for discrete treatments or make partially linear or parametric assumptions that may suffer from model misspecification. To alleviate these problems, we extend causal forest (CF) with non-parametric dose-response functions (DRFs) that can be estimated locally using a kernel-based doubly robust estimator. Moreover, we propose a distance-based splitting criterion in the functional space of conditional DRFs to capture the heterogeneity for the continuous treatments. We call the proposed algorithm generalized causal forest (GCF) as it generalizes the use case of CF to a much broader setup. We show the effectiveness of GCF by comparing it to popular uplift modeling models on both synthetic and real-world datasets. We implement GCF in Spark and successfully deploy it into Didi's real-time pricing system. Online A/B testing results further validate the superiority of GCF.

## CCS CONCEPTS

- **Computing methodologies** → *Kernel methods; Classification and regression trees*;
- **Applied computing** → *Decision analysis*;
- **Mathematics of computing** → *Continuous functions*.

## KEYWORDS

Treatment Effect Estimation, Continuous Treatment, Uplift Modeling, Dynamic Pricing

## 1 INTRODUCTION

The ride-hailing platforms such as DiDi, Uber, and Lyft, typically provide app-based travel services for passengers and flexible job opportunities for drivers by matching the transportation demand from passengers with the vehicle supply by drivers. How to maximize the efficiency of these platforms plays an important role in

many ways, such as improving the income of drivers and facilitating the transition of passengers with high quality. However, it is extremely challenging given the real-time dynamic environment of these ride-hailing platforms. In a short period of time, the number of idle drivers in a given area can be seen as a constant since vehicle re-positioning takes time. On the other hand, passengers demand can change dramatically and rapidly for a lot of reasons such as price, weather and change of plans. Subsequently adjusting the demand is at the heart of the ride-hailing platforms and often draws more attention [19, 28].

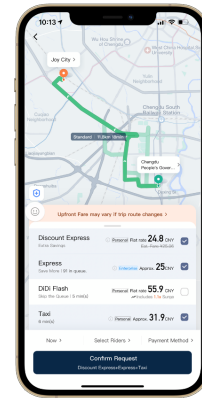
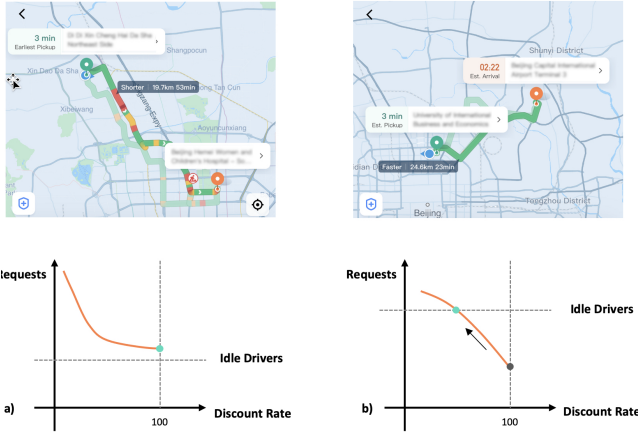


Figure 1: An example on DiDi

DiDi is the world's leading mobility technology platform that offers sustainable and reliable ride-hailing services by connecting over 550 million riders and tens of millions of drivers world-wide everyday. An typical flow of how passengers get a ride on DiDi is shown in Figure 1. Passengers first choose a pick-up location and a destination and then see the estimated price of various ride options and the other trip information. Given the information, passengers may respond by either clicking on the 'Confirm Request' button or ending up with no requests. In DiDi, pricing for trips is at Origin-Destination-Time (ODT) level which guarantees a uniform price for all passengers on the same ODT. To improve DiDi's efficiency by

\*Both authors contributed equally to this research.

adjusting the demand on passengers’ side, pricing with discounts works since requests usually increase with price going down. But this is not a trivial decision to make as a too low price can result in excessive requests and subsequently longer waiting time, henceforth hurting passengers’ experience and downgrading platforms’ efficiency. On the flip side, if the discount rate is too high, it may not be sufficient to stimulate enough requests that can be assigned to idle drivers on the ODT. The fact is that the threshold is determined by how the demand changes with price in which different ODT may significantly differ. In Figure 2, for example, we present how demand varies with price on different ODT. The demand may increase exponentially with discounts on the left and may fluctuate with ups and downs as on the right. Thereby, the same discount for different ODT makes little sense. In other words, the platforms should assign appropriate discounts to ODT accordingly to reach where the ODT would have more vehicle transitions or equivalently the highest increase in total requests, by leveraging ODT’s specific information and real-time supply-demand relationship to identify the impact of discounts on their requests.



**Figure 2: This plot displays different discount strategies at different ODT scenarios. When the demand is over supply, no discount should be charged (left plot), while in the off-peak time, we use discount to stimulate the requests to balance the marketplace.**

More generally, the question is how to estimate the discount effect on demand under different scenarios, formally described as the problem of Heterogeneous Treatment Effect (HTE) estimation in the field of causal inference, which has been of growing interests for decision-makers in a wide spectrum of contexts. It uncovers the effect of interventions at sub-group levels, thereby providing highly tailored suggestions rather than a one-size-fits-all policy. For online marketplace, the treatment is continuous and further have multiple dimensions for ride hailing platforms since multiple travel options can be assigned to discounts as in Figure 1. Considering the causal effect under continuous treatments presents a challenge for the marketplace while maintaining crucial for maximizing its efficiency and performance.

A series of algorithms have been developed to address the problem of HTE estimation. The earliest solution can date back to when

uplift modeling had most appeals as in [25] and recently adoptions in online marketplaces such as [15, 31]. However, these implementations fail to discuss how to mitigate confounding bias which is prevalent in observational data. In contrast, Statistics and Econometric methods, such as Causal Forest (CF) [1] directly consider the relationship among outcome and treatment in presence of confounding variables. However, the theoretical property of the estimators is built on the assumption that the outcome is partially linear in the treatments. Generally speaking, in practice the effect of discounts on requests can be any function of treatments, as illustrated in Figure 2. It remains unexplored proposing an estimator for HTE under no linear or parametric assumptions with theoretical guarantees. Meanwhile, the scalability of an algorithm is key to its deployment into the real world, by increasing which we can gain faster hyperparameter tuning, potential variance reduction with more data, and algorithm advancement. Algorithms on single-machine systems limits its application to the online marketplace with massive data such as tremendous trajectories of 550 million riders on DiDi. In recent years, neural network based methods, such as are also been developed [23, 27], but it lacks interpretability which is important in the high stake settings like pricing strategy.

In this paper we overcome the challenges aforementioned by proposing a large-scale distributed algorithm that provides HTE estimations for multiple dimensional continuous treatments with a theoretical guarantee. To summarize, our main contributions are

- We fully examine the problem of HTE estimations and leverage the possible information among the outcome and the treatment and covariates to do counterfactual predictions, instead of the ones through traditional uplift modeling. Additionally, our tree-based algorithm avoids weak interpretability compared to deep learning models since it shows feature importance of expert-specific features, which in turn guide future high-level decision-makings, and provides the curve estimation of how demand changes with price.
- We relax the partially linear model assumption on demand curve that is often required by prevailing algorithms for HTE estimations such as CF and provide a tree-based model-free algorithm that leads to doubly robust estimators through combining general non-parametric Dose Response Functions with nodes splitting. Specifically, we propose a distance-based splitting criterion for growing trees recursively that guarantees heterogeneity, which quantifies the difference between the non-parametric DRF of child nodes.
- Our proposed GCF has shown its two advantages over the existing baselines on off-line datasets, such as synthetic datasets and large-scale real-world datasets, and demonstrated its high performance on online deployment at DiDi. First, it improves on SOTA in terms of multiple evaluation metrics with more accurate predictions. Second, We implement GCF on Apache Spark MLlib and obtain higher computational efficiency by distributed computing, which guarantees a wide application to ride-hailing platforms.

The rest of the paper is organized as follows. In Section 2, we review related works in the existing literature. Section 3 introduces preliminary notations and backgrounds. Then in Section 4, we formally propose GCF. We validate the performance of GCF by applying

it to both synthetic and real-world datasets in Section 5. Finally, in Section 6, the practical effectiveness of GCF is demonstrated by its superior performance in an online experiment. The Spark implementation of GCF is also briefly introduced in this section. We conclude the paper with some discussions in Section 7.

## 2 RELATED WORKS

A growing amount of literature has been working on addressing the problem of HTE estimation with continuous treatments. By its definition, HTE can be estimated through directly modeling the uplift of the outcome on interventions as is known as Uplift Modeling [30]. The well-known methods include Meta-Learner [18], Causal Inference Tree [29] and deep learning-based approach [20]. However, uplift modeling suffers from severe biases without completely leveraging the information between the outcome and treatments and covariates and it highly depends on the outcome given no treatments.

In view of that, CF, for instance, introduce the concept of score function that describes how outcome itself varies with treatments and covariates and adapts Random Forest for regression problems to HTE estimation. Specifically, they propose a general score function as the objective of the optimization problem, the solution of which leads to HTE estimators. And they proceed with developing the GRF algorithm as a modification of random forest, which utilizes a subset of training samples for growing trees by recursively partitioning via a splitting criterion associated with the estimand of interest. And the final estimator is given by a weighted average over the outcomes of the remaining training samples, known as the honesty principle. The final estimator obtained from CF further exhibits a lower degree of bias by tree ensembles. The validation of these tree-based algorithms highly relies on a considerably strong assumption underlying the score function. Precisely, they assume that the score function or the outcome is linear in the treatment. It reduces the HTE estimation to the estimation of heterogeneous linear coefficient of treatment, resulting in a splitting criterion computed by the difference between the slopes of linear models regressing on treatment. Nevertheless, general HTE estimation may go beyond linear assumes in CF and Orthogonal Random Forest [24] or parametric models utilized in Bayesian Addictive Regression Trees [11]. In this paper, we claim an estimator under no linear assumptions on the score function and generalize the heterogeneous coefficient of a linear model to an operator on treatment utilizing non-parametric Conditional Dose-Response Function (CDRF). The splitting criterion is then proportional to the distance in the functional space of CDRF as a proxy for heterogeneity, instead of the difference in two points.

Another line of work is to estimate Dose-Response Function (DRF), in the presence of confounding bias and regression bias or both. For example, DRF combined with IPW [9, 32] can achieve consistent estimators by weighting the estimation with the probability density of treatment and [7] model DRF as non-parametric functions using kernel regression. To advance, [17] propose doubly robust estimators for DRF by combining the estimation of generalized propensity score with the estimation of outcome using kernel regression. However, they cannot handle massive amounts of high-dimensional data. Recently, kernel-based DML [2] estimates the

nuisance functions with cross-fitting, constructs a non-parametric Doubly Robust estimator for DRF by Gaeutax Derivative, and shows the asymptotic normality. But these approaches only serve for DRF estimations without considering heterogeneity. In other words, the estimator for DRF that is asymptotically unbiased does not guarantee the one for HTE. In this paper, we propose a non-parametric doubly robust estimator of CDRF and its by-product is the HTE estimators.

## 3 PRELIMINARIES

### 3.1 Notations and Assumptions

We formally introduce the notations for HTE estimation with continuous treatments. Following the potential outcome framework in [22, 26], we let  $T$  be the  $d_t$ -dim continuous treatment,  $X = (X^j)_{j=1}^{p_X}$  be the  $p_X$ -dim confounding variables,  $U$  be the  $p_U$ -dim outcome-specific covariates,  $Z$  be the  $p_Z$ -dim treatment-specific covariates independent of  $U$ , and  $Y$  be the outcome of interest. The population  $\Omega = (X, U, Z, Y, T) \in \mathbb{R}^{p_X+p_U+p_Z+1+d_t}$  satisfies

$$Y = g(T, X, U) + \epsilon; T = f(X, Z) + v$$

where  $\epsilon, v$  are noises of zero mean and  $g: \mathbb{R}^P \times \mathbb{R} \rightarrow \mathbb{R}$

and  $f: \mathbb{R}^P \rightarrow \mathbb{R}$ .

And  $\{(X_i, U_i, Z_i, Y_i, T_i), i = 1, \dots, n\}$  denote i.i.d. samples drawn from  $\Omega$ . In practice, the decomposition of  $X, U, Z$  from observed covariates is difficult or even infeasible. Therefore, without additional specifications, we use  $X$  as a summary of observed covariates for simplicity throughout the paper. The potential outcome under treatment  $t$  is  $Y_{(t)}$ . Recall that Propensity Score (PS) [26] for a discrete treatment is  $P(T = t|X)$ , the probability for a unit receiving treatment  $t$  given the covariates  $X$ . In the context of continuous treatments, [13, 26] introduce Generalized Propensity Score (GPS) which is the probability density function  $\pi(T = t|X)$ .

Our estimand of interest is CATE  $\theta(t, X)$ , formally defined as

$$\theta(t, X) = E[Y_{(t)}|X] - E[Y_{(0)}|X]$$

To identify  $\theta(t, X)$ , common assumptions as in [14, 17], i.e. Assumption 1-3, are made throughout the paper.

**Assumption 1. Consistency:**  $E[Y|T = t] = E[Y_{(t)}|T = t]$ , i.e. the outcome of any sample solely depends on its treatment.

**Assumption 2. Ignorability:** The potential outcomes  $Y_{(T)}$  is independent of treatment  $T$  given covariates  $X$ .

**Assumption 3. Positivity:** The GPS  $\pi(T = t|X) > p_{min} > 0, \forall t, X$ , i.e. the density for any sample receiving any treatment is bounded away from 0.

Under the above assumptions, we have

$$\begin{aligned} \theta(t, X) &= E[Y_{(t)}|X] - E[Y_{(0)}|X] = E[Y|T = t, X] - E[Y|T = 0, X] \\ &= E[g(t, X)|T = t, X] - E[g(t, X)|T = 0, X] \end{aligned}$$

where the first equality holds by Assumption 1 and the second equality holds by Assumption 2. Positivity is indispensable for the conditional expectation to be well-defined in the last line whereas being too strong. In practice, it can be reduced to a weak version.

**Assumption 4.** *Weak Positivity: The variance of GPS  $\sigma(\pi) > \sigma_{min} > 0, \forall t, X$  where*

$$\sigma(\pi) = \int_t t^2 \cdot \pi(T = t|X) dt - \left( \int_t t \cdot \pi(T = t|X) dt \right)^2.$$

### 3.2 Dose-Response Function

For continuous treatments, the treatment effect can be fully characterized by Dose-Response Function (DRF) which is formally defined as a function of  $t$

$$\mu(t) := E[Y|T = t]$$

Generally speaking, DRF can be either parametric or non-parametric and herein we give it to any function of  $t$  as a substantial generalization of the existing tree-based methods. The estimand of interest related to DRF heavily depends on the contexts [8], such as treatment effect  $(E[Y(t)] - E[Y(0)])$ , partial effect by its definition  $\left( \frac{E[Y(t_2)] - E[Y(t_1)]}{t_2 - t_1} \right)$  and elasticity  $\left( \frac{\partial \log(E[Y(t)])}{\partial \log(t)} \right)$ . Specifically, conditional DRF (CDRF)

$$\mu(t, X) = E[Y|T = t, X]$$

characterizes the outcome with interventions at individual or subgroup levels which grants dedicate access to heterogeneous treatment effect and thereby being the main quantity of interest, since

$$\theta(t, X) = \mu(t, X) - \mu(0, X).$$

**Remark 1.** *Moreover, the CDRF at subgroup levels can be a proxy for DRF with respect to the samples in the subgroup. In other words, the estimation of CDRF can be transitioned to DRF estimations in certain scenarios, such as in the context of estimators given by two groups of samples in different child nodes. In what follows, we give dedicate details to non-parametric DRF estimations.*

### 3.3 Kernel Regression and Double/Debiased Estimators

For general non-parametric function approximations, kernel regression [6] works with solid theoretical foundations. Precisely, to model the non-parametric relationship  $y = g(x) + \epsilon$  given data  $(X_i, Y_i)$ , kernel regression with linear kernel smoother gives it to the estimator

$$\hat{g}(x) = \frac{\sum_{i=1}^n K_h(x, X_i) \cdot y_i}{\sum_{i=1}^n K_h(x, X_i)}$$

where  $K_h(x, X_i)$  is a scaled kernel density with  $h$  being the bandwidth for smoothness. Typical choices of kernel include Uniform, Epanechnikov, Biweight, Triweight and Gaussian.

We obtain an asymptotically unbiased estimator by combining the vanilla kernel regression and doubly robust estimators. Formally, the estimator for DRF  $\mu(t)$  is proposed as

$$\hat{\mu}(t) = \frac{1}{n} \cdot \sum_{i=1}^n \hat{\mu}(t, X_i) + \frac{K_h(T_i, t)}{\hat{\pi}(\mu(t|X_i))} \cdot (Y_i - \hat{\mu}(t, X_i)).$$

which can be estimated by two-stage estimation, such as kernel-based DML method as proposed in [2]. First, we estimate the CDRF  $\mu(t, X)$  with  $\hat{\mu}(t, X)$  and the GPS  $\pi(T = t|X)$  with  $\hat{\pi}(t|X)$  by means of various machine learning methods with or without cross-fitting technique. Then, with the nuisance estimators plugged in, kernel-based double/debiased estimator is explicitly derived.

## 4 GENERALIZED CAUSAL FOREST

In this section, we formally present the details of our algorithm, GCF. Building on CF, GCF further relaxes the linear assumption on DRF by considering general non-parametric DRF which leads to a splitting criterion that can be estimated using kernel-based doubly robust estimator as described in the previous section. In what follows, we give it to a workflow of GCF at both the training stage and prediction stage, followed by the elaborations on the splitting criterion, estimators, and practical tweaks for the numerical implementation.

---

### Algorithm 1: Generalized Causal Forest

---

**Input** dataset  $O = (X_i, T_i, Y_i), i = 1, \dots, n$ ; number of trees  $B$ ; number of features sampled for growing a tree  $mtry$ ; the minimum sample size on each leaf node  $min.node.size$ ; honesty fraction  $\alpha$ ; tolerance  $\tau$ ; positivity threshold  $\zeta$ ;

#### Trainings begin

Data  $O_1$  and data  $O_2$  by a  $(\alpha, 1 - \alpha)$  split rule applied to  $O$  for honesty;

Pre-train outcome regression model  $\hat{\mu}$  and treatment density estimation  $\hat{\pi}$  on sample  $\Omega_1$ ;

$b \leftarrow 1$ ;

**while**  $b \leq B$  **do**

Randomly sample a feature set  $X^S$  of size  $mtry$  from  $X$ ;

**for** *The stopping rule is not satisfied* **do**

Identify each parent node  $P$ ;

Compute the splitting criterion  $\Delta(\cdot)$  (3) over the samples in  $O_1$  with  $X^S$ ;

Grow the tree  $\mathcal{T}_b$  by splitting at the parent node  $P$  according to the  $\Delta(\cdot)$ ;

**end**

Assign samples in  $O_2$  to leaf nodes based on  $\mathcal{T}_b$  and let  $b \leftarrow b + 1$ ;

**end**

**end**

**Output** Causal forest with  $B$  trees by recursive partitioning on  $X$ ; node assignments for samples in  $O_2$ ;

#### Predictions begin

CDRF estimation  $\hat{\mu}_b(t, \mathbf{x})$  by the local weighted average over the outcomes of samples in  $O_2$  that falls into

$$\mathcal{L}_b(\mathbf{x}) \text{ as } \sum_{i=1}^n \frac{1_{X_i \in \mathcal{L}_b(\mathbf{x})} \cdot 1_{T_i=t} \cdot Y_i}{|\mathcal{L}_b(\mathbf{x})|}; \text{ CATE}$$

estimation  $\hat{\theta}_b(t, \mathbf{x}) = \hat{\mu}_b(t, \mathbf{x}) - \hat{\mu}_b(0, \mathbf{x})$  and

$$\hat{\theta}(t, \mathbf{x}) = \frac{1}{B} \sum_{b=1}^B \hat{\theta}_b(t, \mathbf{x});$$

**end**

---

Let the number of trees be  $B$  and then GCF grows trees  $\mathcal{T}_b, b = 1, \dots, B$ , by repeating the tree-growing process  $B$  times through bootstrapping. At the training stage, we construct the tree  $\mathcal{T}_b$  by recursive partitioning based on maximizing the splitting criterion  $\Delta(c_1, c_2)$ . It is proportional to the discrepancy between the CDRF  $\theta$  given by the left and right child nodes, respectively, and thereby being an accurate approximation to the underlying heterogeneity.

Each time we maximize the splitting criterion, we are maximizing the heterogeneity of leaf nodes within a tree and thereby guaranteeing an estimator for CDRF that exhibits good theoretical properties at the prediction stage. We elaborate on this splitting criterion both in practical sense and theoretical sense in the next part.

Our algorithm is implemented on Apache Spark for large-scale data processing and the mechanism of the tree-growing process is different from that in CF. To elucidate on that, the data is stored at the master machine and trees are copied to each branch machine. Then data is randomly distributed to branch machines for the computation and collected back to the master machine for the final criterion that is used for updating a tree. The updated tree will be copied to each branch machine again and we repeat the process until the tree stops splitting. This distributed computation and clustered storage leverage the computational power of multiple machines for speeding up the training process. We refer readers to the appendix for more information on GCF's Spark implementation.

The splits in the tree-growing process terminate when various pre-specified stopping criteria are met, for example, when the sample size of child nodes is smaller than the parameter *min.node.size* or the splitting criterion  $\Delta(c_1, c_2)$  is smaller than *min.info.gain*  $\tau$ .

We also follow the honesty principle first proposed in [1] by partitioning the training samples into two parts where one is for constructing the tree and the other is for estimating CATE on the leaf nodes. That is to say that each training data can either be utilized to estimate CATE or contribute to growing a tree. At the prediction stage, the leaf node of given samples  $\mathbf{x}$  on each tree  $\mathcal{T}_b$  is denoted by  $\mathcal{L}_b(\mathbf{x})$ . The estimation of CDRF  $\hat{\mu}_b(t, \mathbf{x})$  on  $\mathcal{L}_b(\mathbf{x})$  takes a local weighted average on training samples in  $\mathcal{L}_b(\mathbf{x})$ , with weight  $\alpha_i$  being

$$\alpha_i = \frac{\sum_{i=1}^n 1_{X_i \in \mathcal{L}_b(\mathbf{x})} \cdot 1_{T_i=t} \cdot Y_i}{|\mathcal{L}_b(\mathbf{x})|}. \quad (1)$$

Accordingly, the CATE estimator on each tree  $b$  is given by  $\hat{\theta}_b(t, \mathbf{x}) = \hat{\mu}_b(t, \mathbf{x}) - \hat{\mu}_b(0, \mathbf{x})$ . The final CATE estimation is the average of  $\mathcal{L}_b(\mathbf{x})$  over  $B$  trees, as  $\hat{\theta}(t, \mathbf{x}) = \frac{1}{B} \sum_{b=1}^B \hat{\theta}_b(t, \mathbf{x})$ .

## 4.1 Splitting Criterion

Given a parent node  $P$  and training samples with covariates  $\mathbf{X}_\omega$ , our splitting criterion  $\Delta(c_1, c_2)$  is proposed as

$$\Delta = \frac{n_{C_1} n_{C_2}}{n_P} \cdot \|\hat{\theta}_{C_1} - \hat{\theta}_{C_2}\|_F^2 = \frac{n_{C_1} n_{C_2}}{n_P} \cdot D(\hat{\theta}_{C_1}, \hat{\theta}_{C_2}) \quad (2)$$

where  $\hat{\theta}_{C_1}, \hat{\theta}_{C_2}$  are the CATE estimators in the Banach space of  $\theta_x$ , respectively. The sample sizes of parent node, left child node and right child node are  $n_P, n_{C_1}$  and  $n_{C_2}$ , respectively. The ratio  $\frac{n_{C_1} n_{C_2}}{n_P}$  in  $\Delta(c_1, c_2)$  is to balance the sample sizes between the two child nodes. Distance metric  $D$  measures the distance between  $\hat{\theta}_{C_1}$  and  $\hat{\theta}_{C_2}$  in the Banach space  $\{h : \mathcal{R}^{d_t} \rightarrow \mathcal{R}\}$ , which is to be maximized in the splitting so as to optimize the heterogeneity. Some commonly used metrics [4] are  $D_1 = \int_t |\hat{\theta}_{C_1}(t) - \hat{\theta}_{C_2}(t)| dt, D_2 = \int_t |\hat{\theta}_{C_1}(t) - \hat{\theta}_{C_2}(t)|^2 dt, D_\infty = \max_t |\hat{\theta}_{C_1}(t) - \hat{\theta}_{C_2}(t)|$  by adopting  $L_1, L_2$  and  $L_\infty$  norms, respectively. We next show how to estimate CDRF  $\hat{\theta}_{C_1}$  and  $\hat{\theta}_{C_2}$  using kernel-based doubly robust estimator as in [2].

## 4.2 CATE Estimation

The estimation for DRF is a precondition for the estimation of the splitting criterion. In this paper, we point out kernel-based DML estimator in [2] can be adapted to the DRF estimation in our GCF and guides the tree splitting.

Recall that, the DML estimation for DRF is given by

$$\hat{\mu}(t) = \sum_{i \in C} \left( \hat{\mu}(t, X_i) + \frac{K_h(T_i - t)}{\hat{\pi}(t|X_i)} \cdot (Y_i - \hat{\mu}(t, X_i)) \right)$$

where  $\hat{\mu}(t, X_i)$  is the pretrained estimator for  $\mu(t, X)$  at  $X_i$ ,  $\hat{\pi}(t|X_i)$  is the pretrained estimator for GPS at  $X_i$  and  $C$  denotes the child node.

When adapted to our framework, we additionally derive the following estimator for CDRF by innovatively combine kernel regression with Doubly Robust estimators.

*CDRF estimator.* The estimator is given by

$$\tilde{\mu}(t, X_i) = \hat{\mu}(t, X_i) + \frac{K_h(T_i - t)}{\hat{\pi}(t|X_i)} \cdot (Y_i - \hat{\mu}(t, X_i))$$

*DRF and ATE estimator.* The ATE estimator is given by

$$\begin{aligned} \tilde{\mu}(t) &= \frac{\sum_{i \in C_1} \tilde{\mu}(t, X_i)}{|n|} \\ \hat{\theta}_{x \in C_1}(t) &= \tilde{\mu}(t) - \tilde{\mu}(0) \end{aligned}$$

In estimating CATE, the smoothness condition of DRF plays an important role for simplifying the computation. For convex and smooth DRF with  $L_P$  norm, we can approximate the  $\hat{\theta}_{x \in C_1}(t)$  in the splitting criterion with a closed-form  $t \cdot \frac{\partial \tilde{\mu}(t)}{\partial t}$  where  $\hat{\Phi}(t) = \frac{\partial \tilde{\mu}(t)}{\partial t}$  is called PDRF. To see why this holds, by the convexity and specifying  $\|\cdot\|_F$  to be  $L_P$  norm, we have that

$$\Delta \leq \frac{n_{C_1} n_{C_2}}{n_P} \cdot \|\hat{\Phi}_{C_1} - \hat{\Phi}_{C_2}\|_F^2 \cdot (T_{max})^2$$

$$\Delta \geq \frac{n_{C_1} n_{C_2}}{n_P} \cdot \|\hat{\Phi}_{C_1} - \hat{\Phi}_{C_2}\|_F^2 \cdot (T_{min})^2$$

This is being said that  $\Delta$  is equivalent to  $\tilde{\Delta} = \frac{n_{C_1} n_{C_2}}{n_P} \cdot \|\hat{\Phi}_{C_1} - \hat{\Phi}_{C_2}\|_F^2$ , the objective of the optimization problem at the tree splitting in Algorithm 1.

For Gaussian kernels and a one-dimensional treatment,  $\Phi(t)$  is

$$\begin{aligned} \hat{\Phi}(t) &= \frac{\partial \tilde{\mu}(t)}{\partial t} = \frac{\sum_{i=1}^n K'_h(T_i - t) Y_i}{\sum_{i=1}^n K_h(T_i - t)} \\ &= \frac{[\sum_{i=1}^n K_h(T_i - t) Y_i]}{[\sum_{i=1}^n K_h(T_i - t)]^2} \end{aligned}$$

However, for general convex DRF, the PDRF may be discontinuous or even ill-defined. For example, non-differentiable kernel functions like uniform, epanechnikov, biweight and triweight,  $\Phi$  can only be estimated via numerical approximations of  $\Phi(t) = \frac{E[\mu(t + \delta) - \mu(t)]}{\delta}$ .

## 4.3 Asymptotic Property

In what follows, we state the convergence result under mild assumptions. We show that the final estimator for CATE  $\theta_x(t)$  given by our proposed GCF is doubly robust theoretically in the sense

that it is asymptotically unbiased when either the estimator for Generalized Propensity Score or the estimator for the outcome is unbiased. Moreover, we establish a point-wise second-order convergence result, which is a special case of Functional Central Limit Theorem (FCLT).

Our theoretical results distinguish from the existing ones in three aspects. First, compared to the results of [16] which only hold for binary treatments, ours allow for continuous treatments. Meanwhile, [16] show the first-order convergence result and we furthermore present a point-wise second-order result. While [1] propose the convergence of the point estimator for the parameter of CATE with continuous treatment, out of the fact that their DRF is presumed to be linear, we estimate the non-parametric CATE and show its convergence in the functional space. Lastly, the doubly robust estimator under no parametric assumptions given by [2] is asymptotically unbiased with respect to ATE, which does not necessarily guarantee a CATE estimator.

Let us start with the required conditions for establishing the theorems.

**Assumption 5.** *The pdf of the joint distribution  $f(x, y, t)$  is three-times differentiable.*

**Assumption 6.** *The second-order symmetric kernel  $k(\cdot)$  is bounded differentiable.*

**Assumption 7.** *Suppose that the estimators  $\hat{\pi}$  and  $\hat{\mu}$  satisfies*

$$\begin{aligned}\sigma_x(\hat{\mu}) &= \int_x (\hat{\mu}(t, x) - \mu(t, x))^2 \cdot f(t, x) dx \xrightarrow{P} 0 \\ \sigma_x(\hat{\pi}) &= \int_x (\hat{\pi}(t|x) - \pi(t|x))^2 \cdot f(t, x) dx \xrightarrow{P} 0 \\ \sqrt{nh} \sqrt{\sigma_x(\hat{\mu})} \cdot \sqrt{\sigma_x(\hat{\pi})} &\xrightarrow{P} 0\end{aligned}$$

where  $\xrightarrow{P}$  means convergence in probability.

**Assumption 8.** *Suppose that  $\psi_{\theta_x, v(x)}$  is Lipschitz in  $\theta_x$  and  $\theta_x$  is Lipschitz in  $x$  and  $\|\theta_x\| \leq C$  for some constants  $C$ .*

**Assumption 9.** *Suppose that  $\psi_{\theta_x, v(x)}$  is twice continuously differentiable in  $\theta(x)$  and  $\theta(x)$  is convex in  $t$ .*

**Assumption 10.** *Suppose that  $\psi_{\theta_x, v(x)}(\omega_i) = \theta_x(T_i) - Y_i + v(x)$  is a negative gradient of a convex function and the expected score function  $E[\psi_{\theta_x, v(x)}(\omega_i)]$  is a negative gradient of a strongly convex function.*

We first show that the doubly robust estimator for DRF and ATE is asymptotically unbiased which is crucial for the theoretical guarantee of the successive estimators for CDRF and CATE.

**Lemma 1.** *Let Assumptions 1-3 and 5-7 hold. Then the doubly robust estimator  $\tilde{\mu}$  is asymptotically Gaussian in the sense that for any given  $t$ ,*

$$\begin{aligned}\sqrt{nh^{d_t}} (\tilde{\mu}(t) - \mu(t)) &\rightarrow N(0, V_t^1), \\ \tilde{\mu}(t) - \mu(t) &\xrightarrow{P} 0\end{aligned}$$

where  $V_t^1 = E \left[ \frac{\text{var}(Y|T=t, X=x)}{\pi(t|x)} \right] \cdot \int_{-\infty}^{\infty} k(u) du < \infty$  as in [2].

**PROOF.** It is straightforward to check that all the assumptions in [2] hold when utilizing the optimal bandwidth  $h$  that satisfies

$$h^2 \sqrt{nh^{d_t}} \rightarrow 0.$$

Then we close the proof by directly following the result in [2].  $\square$

**Corollary 1.** *According to Slutsky's theorem, we have that*

$$\tilde{\mu}(t) - \tilde{\mu}(0) - (\mu(t) - \mu(0)) \xrightarrow{P} 0$$

Now we prove that the estimated CATE actually converges to the ground truth in the functional space by customizing the above ATE estimator to a tree-based schema. The unbiased property and asymptotically normality are summarised as Theorem 1 of which the proof is in Appendix and Conjecture 1, respectively.

**Theorem 1.** *Let Assumptions 1-3 and 5-10 hold. Then the final estimator  $\hat{\theta}_x(t)$  given by the proposed GCF converges to CATE  $\theta_x(t)$  in the functional space as the number of samples  $n \rightarrow \infty$ , i.e.*

$$\left\| \hat{\theta}_x(t) - \theta_x(t) \right\|_F \rightarrow 0 \text{ as } n \rightarrow \infty.$$

**Corollary 2.** *The convergence can be of any form depending on the chosen norm of  $\|\cdot\|_F$ . For example, the result is  $L_p$  convergence when  $F$  is  $L_p$  with  $1 < p < \infty$  and will be uniform convergence when  $F$  is  $L_\infty$ .*

**Conjecture 1.** *The central limit theorem with respect to a function is often denoted by Functional Central Limit Theorem (FCLT). This is a generalization of point-wise asymptotic Gaussian as stated in [1]. Formally, under Assumptions 1-3 and 5-10 and when  $\|\cdot\|_F$  is chosen to be  $L_\infty$ , we have that for any  $t$ ,*

$$\frac{\hat{\theta}_x(t) - \theta_x(t)}{\sigma_x(t)} \rightarrow \mathcal{N}(0, 1), \text{ as } n \rightarrow \infty$$

**Conjecture 2.** *We point out that the FCLT result can still hold when  $F$  is general functional norm which serves as a conjecture here. The proof should be a combination of stochastic analysis of the stochastic process  $\theta_x(t)$  and large-scale approximations. This goes beyond the scope of this paper and we defer the proof to future work.*

## 4.4 Practical Considerations

In the work of [17], they claim that the choice of bandwidth  $h$  for kernels weighs more than the choice of density functions, since  $h$  deals with the trade off between bias and variance. Usually, a small  $h$  avoids a large variance while a large  $h$  reduces the bias. The empirical ways of choosing an optimal  $h$  are Cross Validation and Rule-of-thumb [3].

When utilizing kernel densities for weighting, we often suffer from the boundary bias if without normalization. To this end, we normalize estimators with the cumulative density function of range  $[T_{min}, T_{max}]$  of treatments. More specifically, the estimators are divided by  $\int_{T_{min}}^{T_{max}} K_h(T_i - t) dt$ .

Regarding the positivity assumption in practice, we use a hyperparameter  $\zeta$  to control for a strictly positive variance of GPS  $\sigma(\pi)$ . This is also a guarantee on the weak assumption as stated in Assumption 4. Formally, our proposed splitting criterion is extended to a regularized one as

$$\Delta(c_1, c_2) = \frac{n_{C_1} n_{C_2}}{np} \cdot D(\hat{\theta}_{C_1}, \hat{\theta}_{C_2}) + \zeta \cdot \sigma(\hat{\pi}), \quad (3)$$

where  $\hat{\pi}$  is the estimated GPS. With this additional term, the splitting will tend to maximize the variance of GPS and hence taking the variety of treatments across samples into account.

## 5 EXPERIMENT

In this section, we conduct detailed experiments to validate GCF performance and demonstrate its effectiveness on both synthetic data and real-world datasets.

### 5.1 Evaluation

In what follows we introduce the evaluation metrics on both synthetic and real-world datasets. For the evaluation on synthetic data with known groundtruth, we follow the tradition of regression problems. However, the counterfactual groundtruth is often black-box in real world. We use Qini Curve to do model evaluation accordingly.

*Synthetic Data.* We use PEHE [12] and RMSE to evaluate models, as are commonly used in regression problems. Formally, let  $n$  be the number of treatment groups,  $\hat{\theta}_i^t$  and  $\theta_i^t$  be the predicted and true treatment effect of  $i_{th}$  sample at treatment  $t$ ,  $\hat{\theta}^t = \sum_{i=1}^n \hat{y}_i^t - \hat{y}_i^0$ ,  $y_i^0$  be the reference outcome that is pre-determined. PEHE, RMSE, and ADRF are  $\frac{\sum_{i=1}^n (|\hat{\theta}_i^t - \theta_i^t|)}{n}$ ,  $\sqrt{\frac{\sum_{i=1}^n (\hat{\theta}_i^t - \theta_i^t)^2}{n}}$ ,  $y(\hat{t}) = \int_x \hat{\mu}(t, x) dx$ .

*Real-world Datasets.* We refer readers to [10] for the formal definition of Qini Score and Qini Curve. In practice, a larger Qini Score indicates that model has better performance in identifying HTE.

### 5.2 Model Setups

The baselines for GCF include RF, CF, and Kennedy [17] of which the hyper-parameters are presented in Appendix.

*GCF.* We implement the proposed GCF on Apache Spark MLlib [21] with kernel-based DML estimator, denoted by GCF. For the implementation of GCF, we fix the distance metric  $D$  to be  $d_2$  out of simplicity. The number of trees, the minimum node size and other hyperparameters are set to match those in RF and CF.

RF is a forest-ensemble method without controlling confoundedness. CF makes the partially linear assumption on DRF. Kennedy is a non-parametric doubly robust algorithm but uses a normal splitting criterion. The comparisons inclusively validate our algorithm for both non-parametric DRF estimation and specially designed splitting criterion.

### 5.3 Simulation

Here we show a comprehensive simulation study on synthetic data. First, we elaborate on the data generating process. It is followed by the details of model implementations. Finally we illustrate the numerical results that consistently show the superior performance of our GCF.

*5.3.1 Data Generating Process.* Let  $n$  denote the number of samples and  $p = p_X + p_U + p_Z$  be the dimension of covariates. The covariate matrix is  $(X_i^j)_{i=1, \dots, n}^{j=1, \dots, p_X} = (X_1, \dots, X_n) \in \mathbb{R}^{n \times p_X}$ . Data generating

process (DGP) is

$$Y = \mu(T) + 0.2(X^1 \cdot X^1 + X^4)T + X \cdot \beta_X + U \cdot \beta_U + \epsilon$$

$$T = 20 \cdot \Psi(\phi(X \cdot \beta_X + Z \cdot \beta_Z)) + \nu$$

where  $\phi$  is the sigmoid function and  $\Psi$  is the pdf of Beta distribution. Here we set DRF  $\mu$  to be polynomial(Poly), exponential(Exp), and sinusoidal functions(Sinus).

The above DGP gives us a total of 6 datasets by considering every possible combination of 3 DRFs  $\mu(t)$  and 2 setups of covariate matrix  $\Sigma$ . Noises  $\epsilon, \nu$  follow  $Unif(-1, 1)$ . The Covariates  $X$  and coefficients  $\beta$  follow  $N(0, I_{p_X})$ . We also allow sparsity in the covariates by randomly setting some of the coefficients to 0. Testing datasets are generated with randomly assigned treatments to allow unbiased evaluation.

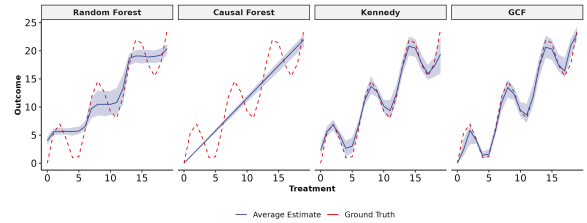


**Figure 3: Comparison of ADRF estimates for RF, CF, Kennedy and GCF. DRF follows sinusoidal pattern. Blue line denotes model average estimations. Confidence bounds of model estimates generated by multiple simulation run are marked in light-blue shade. The ground truth of testing dataset is represented in red dash-line.**

*5.3.2 Simulation Results.* Since some models output the final prediction of  $Y(\hat{t})$  and some output the treatment effect  $\theta(\hat{t})$ , we deliberately compute the pseudo outcome  $Y(\hat{t}) = Y(t) - Y(0)$  as the label in the purpose of the comparability across baselines. The simulation results of 3 datasets are summarized in Table 1 and those of the other 3 datasets are in Appendix. Here PEHE and RMSE are averaged and standard deviations of the metrics across simulation runs are also reported. Overall, GCF significantly outperforms baseline methods, which again validates the superiority of the newly proposed algorithm. More specifically, GCF exhibits the smallest biases across multiple DGP setups of which we refer a comprehensive study to the supplementary.

Additionally, we compare the ADRF curves given by different models with that from the ground truth. An example of ADRF under a DGP specification is shown in Fig. 3. Among those models, the curve of our proposed GCF is closest to the ground truth with a non-linear shape.

### 5.4 Real-world Datasets

Our method is also implemented on real-world datasets of size 10,698,884 which sourced from a ride-hailing platform. A discount that randomly sampled from 6 distinct values  $\{d_0, d_1, d_2, d_3, d_4, d_5 : d_0 < d_1 < \dots < d_5\}$  is assigned to an ODT. The effect of discount on the demand of ODTs is of our primary interests. We apply GCF to

**Table 1: Simulation results on datasets with different DRFs where number of samples  $n = 1000, p_X = 50, p_Y = 5, p_Z = 5$ . Standard deviations are in parenthesis over 100 simulations.**

Methods	Polynomial		Sinusoidal		Exponential	
	PEHE	RMSE	PEHE	RMSE	PEHE	RMSE
RF	5.63(0.4)	4.61(0.3)	4.27(0.4)	3.21(0.2)	3.57(0.4)	2.62(0.2)
CF	14.09(0.4)	12.58(0.4)	5.15(0.4)	3.96(0.2)	4.34(0.3)	3.37(0.2)
Kennedy	4.37(0.5)	3.36(0.5)	4.14(0.5)	2.78(0.3)	3.86(0.4)	2.54(0.2)
<b>GCF</b>	<b>4.14(0.3)</b>	<b>2.88(0.2)</b>	<b>4.05(0.4)</b>	<b>2.7(0.3)</b>	<b>3.85(0.4)</b>	<b>2.48(0.2)</b>

this dataset and evaluate the performance of models by computing Qini Scores.

**Table 2: Qini scores of models under different treatments**

Methods	$d_5$	$d_4$	$d_3$	$d_2$	$d_1$
Xgboost	0.253	0.171	0.177	0.206	0.177
CF	0.253	0.194	0.202	0.272	0.300
<b>GCF</b>	<b>0.309</b>	<b>0.248</b>	<b>0.305</b>	<b>0.444</b>	<b>0.780</b>

The Qini scores of different models are summarized in Table 3. The performance of GCF is superior than the other models as GCF has the highest Qini scores across all levels of discounts.

## 6 IMPLEMENTATION AND DEPLOYMENT

In this section, we demonstrate the superior performance of GCF by conducting an online A/B testing on a real-time pricing system where we deploy the implemented algorithm and baseline methods. We implement GCF on Spark by utilizing the parallel computing environment and open APIs on Spark and we refer the elaborations to the Appendix.

The deployment of models in the DiDi’s online pricing system can be loosely partitioned into two parts (offline and online) as illustrated in Figure 4. In the offline module, the model is trained on historical data to provide HTE estimation that policy optimizer need to generate ODT-level discount strategy. Then generated policy is deployed online and evaluated by the online A/B experiments. In the end, trip logs are anonymously collected to offline database and ready for the next iterations of updates. In what follows, we show the detailed online results of GCF versus the baseline.

We conduct online A/B testings by first splitting ODTs randomly into two groups. The evaluation metric of the online experiment is the finish order (FO) increment. The numerical results of GCF and CF are presented in Table 3. GCF improves on CF by 15.1% and 25.2%, given discounts on one travel option and two travel options, respectively, i.e. one-dimensional treatment and two-dimensional treatment, by taking non-linearity relationship into account. It shows that the more complicated or more general the treatment is, the more efficient the model is, which again shows the superiority of our novel combination of DRF and CF for continuous treatment.

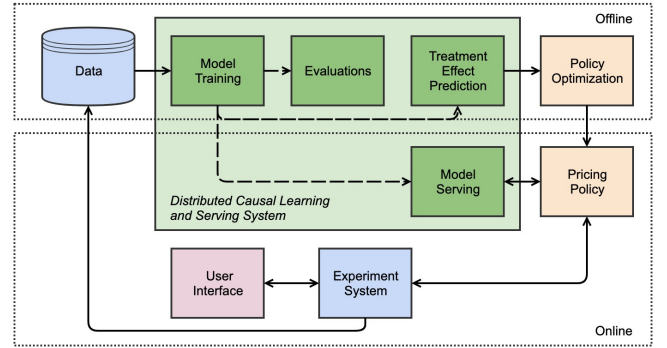


**Figure 4: DiDi’s Online Pricing System**

**Table 3: The improvements of GCF on CF in the scenarios with one travel option and two travel options**

Treatment	FO Improvement
<b>Discount on one travel option</b>	<b>15.1%</b>
<b>Discount on two travel options</b>	<b>25.2%</b>

## 7 CONCLUSION

In this paper, we propose a novel forest-based non-parametric algorithm to address the problem of HTE estimation with continuous treatments. Under the situation that a fully non-parametric and localized ML-based algorithm has not been proposed yet, we extend Causal Forest with a DRF-based splitting criterion computed by the distance in the functional space of the target CDRF. To estimate this DRF, We use the kernel-based doubly robust estimator to guarantee double robustness that mitigates model misspecifications. We implement GCF on Spark to leverage the computational efficiency and test it on both synthetic data and real-world datasets and compare it with the prior art approaches. The numerical results demonstrate that our method significantly outperforms competing methods.

## REFERENCES

- [1] Susan Athey, Julie Tibshirani, Stefan Wager, et al. 2019. Generalized random forests. *The Annals of Statistics* 47, 2 (2019), 1148–1178.
- [2] Kyle Colangelo and Ying-Ying Lee. 2020. Double debiased machine learning non-parametric inference with continuous treatments. *arXiv preprint arXiv:2004.03036* (2020).
- [3] Khosrow Dehnad. 1987. Density estimation for statistics and data analysis.



- [4] Holger Dette, Kathrin Möllenhoff, Stanislav Volgushev, and Frank Bretz. 2018. Equivalence of regression curves. *J. Amer. Statist. Assoc.* 113, 522 (2018), 711–729.
- [5] ehkennedy. 2017. npcausal. <https://github.com/ehkennedy/npcausal>.
- [6] Jianqing Fan and Irene Gijbels. 2018. *Local polynomial modelling and its applications: monographs on statistics and applied probability 66*. Routledge.
- [7] Carlos A Flores et al. 2007. Estimation of dose-response functions and optimal doses with a continuous treatment. *University of Miami, Department of Economics, November (2007)*.
- [8] Douglas Galagate. 2016. *Causal Inference With a Continuous Treatment And Outcome: Alternative Estimators For Parametric Dose-Response Functions With Applications*. Ph.D. Dissertation.
- [9] Daniel J Graham, Emma J McCoy, and David A Stephens. 2015. Doubly robust dose-response estimation for continuous treatments via generalized propensity score augmented outcome regression. *arXiv preprint arXiv:1506.04991 (2015)*.
- [10] Pierre Gutierrez and Jean-Yves Gérardy. 2017. Causal inference and uplift modelling: A review of the literature. In *International Conference on Predictive Applications and APs*. 1–13.
- [11] P Richard Hahn, Jared S Murray, Carlos M Carvalho, et al. 2020. Bayesian regression tree models for causal inference: Regularization, confounding, and heterogeneous effects (with discussion). *Bayesian Analysis* 15, 3 (2020), 965–1056.
- [12] Jennifer L Hill. 2011. Bayesian nonparametric modeling for causal inference. *Journal of Computational and Graphical Statistics* 20, 1 (2011), 217–240.
- [13] Keisuke Hirano and Guido W Imbens. 2004. The propensity score with continuous treatments. *Applied Bayesian modeling and causal inference from incomplete-data perspectives* 226164 (2004), 73–84.
- [14] Paul W Holland. 1986. Statistics and causal inference. *Journal of the American statistical Association* 81, 396 (1986), 945–960.
- [15] Junhao Hua, Ling Yan, Huan Xu, and Cheng Yang. 2021. *Markdowns in E-Commerce Fresh Retail: A Counterfactual Prediction and Multi-Period Optimization Approach*. Association for Computing Machinery, New York, NY, USA, 3022–3031. <https://doi.org/10.1145/3447548.3467083>
- [16] Edward Kennedy. 2020. Optimal doubly robust estimation of heterogeneous causal effects. (04 2020).
- [17] Edward H Kennedy, Zongming Ma, Matthew D McHugh, and Dylan S Small. 2017. Nonparametric methods for doubly robust estimation of continuous treatment effects. *Journal of the Royal Statistical Society. Series B, Statistical Methodology* 79, 4 (2017), 1229.
- [18] Sören R Künnel, Jasjeet S Sekhon, Peter J Bickel, and Bin Yu. 2019. Metalearners for estimating heterogeneous treatment effects using machine learning. *Proceedings of the national academy of sciences* 116, 10 (2019), 4156–4165.
- [19] Chungsang Tom Lam and Meng Liu. 2017. Demand and consumer surplus in the on-demand economy: the case of ride sharing. *Social Science Electronic Publishing* 17, 8 (2017), 376–388.
- [20] Christos Louizos, Uri Shalit, Joris Mooij, David Sontag, Richard Zemel, and Max Welling. 2017. Causal Effect Inference with Deep Latent-Variable Models (*NIPS’17*). Curran Associates Inc., Red Hook, NY, USA, 11 pages.
- [21] Xiangrui Meng, Joseph Bradley, Burak Yavuz, Evan Sparks, Shivaram Venkataraman, Davies Liu, Jeremy Freeman, DB Tsai, Manish Amde, Sean Owen, et al. 2016. Mllib: Machine learning in apache spark. *The Journal of Machine Learning Research* 17, 1 (2016), 1235–1241.
- [22] Jersey Neyman. 1923. Sur les applications de la théorie des probabilités aux expériences agricoles: Essai des principes. *Roczniki Nauk Rolniczych* 10 (1923), 1–51.
- [23] Lizhen Nie, Mao Ye, Qiang Liu, and Dan Nicolae. 2021. VCNet and Functional Targeted Regularization For Learning Causal Effects of Continuous Treatments. *arXiv preprint arXiv:2103.07861 (2021)*.
- [24] Miruna Oprescu, Vasilis Syrgkanis, and Zhiwei Steven Wu. 2019. Orthogonal random forest for causal inference. In *International Conference on Machine Learning*. PMLR, 4932–4941.
- [25] Nicholas J Radcliffe. 2007. Using control groups to target on predicted lift: Building and assessing uplift models. *Direct Marketing Analytics Journal* 1, 3 (2007), 14–21.
- [26] Donald B Rubin. 1974. Estimating causal effects of treatments in randomized and nonrandomized studies. *Journal of educational Psychology* 66, 5 (1974), 688.
- [27] Uri Shalit, Fredrik D Johansson, and David Sontag. 2017. Estimating individual treatment effect: generalization bounds and algorithms. In *International Conference on Machine Learning*. PMLR, 3076–3085.
- [28] Matthew H Shapiro. 2018. Density of Demand and the Benefit of Uber. (2018).
- [29] Xiaogang Su, Joseph Kang, Juanjuan Fan, Richard A. Levine, and Xin Yan. 2012. Facilitating Score and Causal Inference Trees for Large Observational Studies. *J. Mach. Learn. Res.* 13, 1 (oct 2012), 2955–2994.
- [30] Weijia Zhang, Jiuyong Li, and Lin Liu. 2021. A Unified Survey of Treatment Effect Heterogeneity Modelling and Uplift Modelling. *ACM Comput. Surv.* 54, 8, Article 162 (oct 2021), 36 pages. <https://doi.org/10.1145/3466818>
- [31] Yan Zhao, Xiao Fang, and David Simchi-Levi. 2017. Uplift modeling with multiple treatments and general response types. In *Proceedings of the 2017 SIAM International Conference on Data Mining*. SIAM, 588–596.
- [32] Yeying Zhu, Donna L Coffman, and Debashis Ghosh. 2015. A boosting algorithm for estimating generalized propensity scores with continuous treatments. *Journal*

## 8 SUPPLEMENTARY MATERIALS

We put the supplementary materials in this section. First, we write all the notations explicitly used both in the main paper and in the supplementary for consistency. With the notations, we show the full proof of Theorem 1. Then we dive into the details of the data generating process for the simulation study. We present the additional simulation results to further show the effectiveness of our proposed method and the specified parameters. We close this section by describing the Spark framework of GCF that enables large-scale instances processing and faster model training.

### 8.1 Notations

We restate the notations that are consistent with the main paper.

Following the potential outcome framework in [22, 26], we let  $T$  be the continuous treatments,  $X = (X^j)_{j=1}^p$  be the  $p_X$ -dim confounder,  $U$  be the  $p_U$ -dim outcome-specific adjustment variable,  $Z$  be the  $p_Z$ -dim treatment-specific adjustment variable, and  $Y$  be the observed outcome. The potential outcomes under treatment  $t$  is  $Y(t)$ . The population  $\Omega = (\Sigma = (X, U, Z), Y, T) \in \mathbb{R}^{p_X+p_U+p_Z+1}$  satisfies

$$Y = g(T, X, U) + \epsilon$$

$$T = f(X, Z) + v$$

where  $\epsilon, v$  are noises of zero mean,

$$\text{and } g : \mathbb{R}^{p_X+p_U} \times \mathbb{R} \rightarrow \mathbb{R} \text{ and } f : \mathbb{R}^{p_X+p_Z} \rightarrow \mathbb{R}.$$

$\{(\Sigma_i, Y_i, T_i), i = 1, \dots, n\}$  are i.i.d. samples drawn from the population  $\Omega$ . Then the covariate matrix  $\Sigma = (\Sigma_i^j)_{\substack{1 \leq j \leq p \\ 1 \leq i \leq n}} = (\Sigma_1, \dots, \Sigma_n) \in \mathbb{R}^{n \times p}$  where  $p = p_X + p_U + p_Z$ . The Generalized Propensity Score is  $\pi(T = t|X)$ , which is the probability density for a unit receiving treatment  $t$  given the covariate  $X$ .

### 8.2 Proof of Theorem 1

**PROOF.** Under assumptions 1-3 and 5-7, we have Lemma 1 hold. With the asymptotically unbiased estimator plugged in to the splitting criterion, now we adapt what are established in [1] to our GCF. We first define the score function in general scenarios with non-linear DRF, which is denoted by  $\psi_{\theta_x, v(x)}(\omega_i) = \theta_x(T_i) - Y_i + v(x)$  on sample  $\omega_i = (T_i, Y_i)$  where  $\theta_x(\cdot) = \mu(t, x) - \mu(0, x) = \mu(t, x) - v(x)$  is the mapping from  $\mathcal{R}^{d_t}$  to  $\mathcal{R}$  or the distance between two points on the dose response curve. Note that the newly defined score function generalizes the parametric  $\theta(x)$  as in  $\theta(x) \cdot T$  to the generic one  $\theta_x(\cdot)$ , i.e. from  $\mathcal{R}$  to  $\{h : \mathcal{R}^{d_t} \rightarrow \mathcal{R}\}$ .

Solving an estimating equation of score function  $\Psi$  is at the heart of the analysis in [1]. While it does not rely on the linear assumption, we can similarly propose an estimating equation as

$$\|\Psi_{\theta, v}\| = \|E[\psi_{\theta, v}(\omega)]\| = 0$$

And the empirical estimating equation gives it to

$$\begin{aligned} & \min_{\theta, v} \left\| \sum_{i=1}^n \alpha_i \cdot \psi_{\theta, v}(\omega_i) \right\| \\ &= \left\| \frac{\sum_i \theta_x(t, \mathbf{x}_i) + v(\mathbf{x}_i)}{s} - \frac{\sum_i Y_i}{s} \right\| \\ &= \left\| \frac{\sum_i \mu(t, \mathbf{x}_i) - \mu(0, \mathbf{x}_i) + \mu(0, \mathbf{x}_i)}{s} - \frac{\sum_i Y_i}{s} \right\| \end{aligned}$$

where  $\alpha_i$  is the weight as defined in (1) and  $s$  is the number of samples with non-zero weights. Here we propose that with  $\tilde{\mu}(t)$ , we can get an asymptotically optimal solution to the empirical equation as in [1] since we have that

$$\begin{aligned} & \left\| \frac{\sum_i \mu(t, \mathbf{x}_i) - \mu(0, \mathbf{x}_i) + \mu(0, \mathbf{x}_i)}{s} - \frac{\sum_i Y_i}{s} \right\| \\ & \xrightarrow{p} \left\| \mu(t) - \mu(0) + \mu(0) - \frac{\sum_i Y_i}{s} \right\| \\ & \approx \left\| \tilde{\mu}(t) - \tilde{\mu}(0) + \tilde{\mu}(0) - \frac{\sum_i Y_i}{s} \right\| \end{aligned}$$

where the first convergence is by SLLN and the second approximation holds by Lemma 1 aforementioned when  $s \geq \sqrt{nh^{d_t}} \rightarrow \infty$ .

To close the proof, we show that by solving the empirical estimating equation that is utilized in the splitting criterion 3, the final estimator for CATE given by the tree is asymptotically unbiased. This is done by generalizing the theorem 1 in [1].

According to Remark 2 and Remark 3, the conditions of existence of solutions as denoted by Assumption 5 and Specification 1 in [1] is met. Meanwhile, the effectiveness of Assumption 8 implies that the score function is Lipschitz and the expect score function is Lipschitz which are stated as Assumption 1 and 3 in [1]. It is easy to check that Assumption 2 in [1] holds when Assumption 9 holds herein. Remark 1 justifies the validity of Assumption 4 in [1]. Lastly, Assumption 6 [1] is guaranteed by Assumption 10 aforementioned. Since Assumption 1-6 and Specification 1 in [1] are met, one can go through the proof steps of theorem 1 [1] line by line with the functional norm and distance, which leads to

$$\left\| \hat{\theta}_x(t) - \theta_x(t) \right\|_F \rightarrow 0 \text{ as } n \rightarrow \infty.$$

**Remark 2. Regularity:**

$$\begin{aligned} \psi_{\theta_x, v(x)}(\omega_i) &= \theta_x(T_i) - Y_i + v(x) \\ &= \lambda(\theta_x, v(x); x) + \eta(g(\omega_i)) \end{aligned}$$

where  $\lambda(\theta_x, v(x); x) = \theta_x(T_i) + v(x)$  and  $\eta = -I$  and  $g(\omega_i) = Y_i$  satisfy the Regularity as Assumption 4 as in [1].

**Remark 3. Existence of Solutions:** The estimators for the nuisance functions are given by [2]. Then under Assumption 1-3 and 5-7, the convergence result as in [2] hold as implied by Lemma 1. That is to say that the estimators  $\hat{\theta}, \hat{v}$  for  $\theta, v$  given by the subsamples on the child node lead to a solution to the optimization problem

$$\min_{\theta, v} \left\| \sum_{i=1}^n \alpha_i \cdot \psi_{\theta, v}(\omega_i) \right\|$$

Since the score function itself is Lipschitz which implies that it is continuous, Weierstrass theorem gives us that the above optimization problem exists a global optimum which implies the  $\sum \alpha_i \cdot M = 0$ . Therefore, Assumption 5 as in [1] hold in our scenario. This is the key step for guaranteeing the effectiveness of doubly robust estimator in the framework of CF.

**Remark 4. Specification 1:** From Lemma 1, we could get that with  $\sqrt{nh^{d_t}}$  samples, the estimator for DRF converges to the ground truth.

Then the number of samples  $s$  can be specified as  $\sqrt{nh^{d_t}}$  and it satisfies  $\frac{s}{n} \rightarrow 0$  and  $s \rightarrow \infty$ . It follows Specification 1 as in [1]

□

### 8.3 Data Generating Process

Recall that the covariate matrix  $\Sigma \in \mathbb{R}^{n \times (p_X + p_U + p_Z)}$

$$\Sigma = (X_i^j, U_i^j, Z_i^j) = (X_1, \dots, X_n, U_1, \dots, U_n, Z_1, \dots, Z_n)$$

and treatment  $T \in \mathbb{R}$  where  $n$  denotes the number of observations and  $p$  is the dimension of covariates. Data generating process (DGP) works as

$$Y = \mu(T) + 0.2(X_1^2 + X_4)T + X \cdot \beta_X + U \cdot \beta_U + \epsilon$$

$$T = 20 \cdot \Psi(\phi(X \cdot \beta_X^* + Z \cdot \beta_Z)) + v$$

where  $\phi$  is the sigmoid function and  $\Psi$  is the pdf of Beta distribution with shape parameters set to 2 and 3. Here we set DRF  $\mu$  as polynomial(Poly), exponential(Exp), and sinusoidal(Sinus).

$$\mu(t) = 0.2 \cdot (t - 5)^2 - t - 5, \text{ Polynomial}$$

$$\mu(t) = \log\left(1 + \frac{\exp(t)}{t + 0.1}\right) - \log(11), \text{ Exponential}$$

$$\mu(t) = 5 \cdot \sin(t) + t, \text{ Sinusoidal}$$

The above DGP gives us a variety of datasets by taking the combination of DRF  $\mu(t)$  and covariate  $\Sigma$  that are specified by  $n, p$  and DRF. Parameter  $\epsilon, v$  are noises following  $N(0, 1)$ . Covariates  $X, U, Z$  follows  $N(0, I)$  and coefficient vector  $\beta$  follow  $[Unif(-1, 1)]$ . Following this rule, we generate 100 rounds. Meanwhile, in test data, we randomly assigned the treatments to make sure unbiased evaluations.

### 8.4 Simulation Results

Here we show a comprehensive simulation study by presenting detailed simulation results that further show the effectiveness of our proposed method.

In addition to the results provided in the main paper, we provide the inclusive results of our simulation study, which covers all 6 datasets from the Data Generating process. The results are summarized in Table 4. Compared to CF [1] that is the benchmark of our generalization, our GCF outperforms it with significantly smaller errors. Compared to Kennedy [17], our algorithm almost enjoys smaller errors except one dataset. Overall, these evidence demonstrates that our GCF is superior than the algorithms for continuous treatments.

Meanwhile, the ADRF curves are inclusively presented here as a validation of our statement that the proposed GCF can better capture the non-linear relationship between the outcome and treatments compared to competing methods. Figure 5–10 are ADRF curves of GCF and baseline methods on different synthetic datasets. Across all the data sets, our proposed GCF performs the best by being the closest to the curve of ground truth.

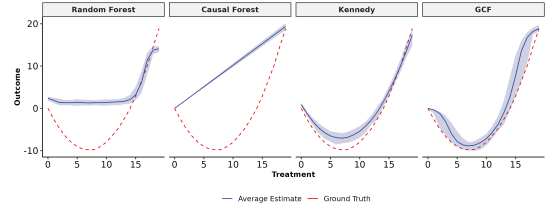


Figure 5: The estimated ADRF curve given by different models where the blue line is the estimation and red dash line is the ground truth on the dataset with DRF being poly and  $n = 1000, N = 100, p_X = 100, p_U = 10, p_Z = 10$

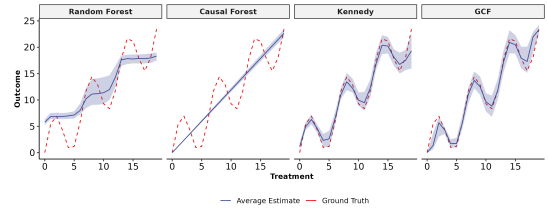


Figure 6: The estimated ADRF curve given by different models where the blue line is the estimation and red dash line is the ground truth on the dataset with DRF being sinus and  $n = 1000, N = 100, p_X = 100, p_U = 10, p_Z = 10$

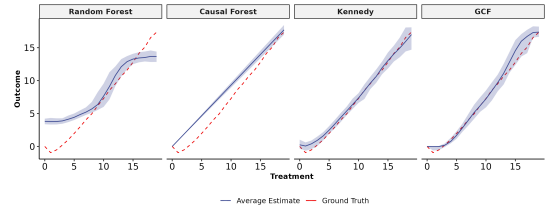


Figure 7: The estimated ADRF curve given by different models where the blue line is the estimation and red dash line is the ground truth on the dataset with DRF being exp and  $n = 1000, N = 100, p_X = 100, p_U = 10, p_Z = 10$

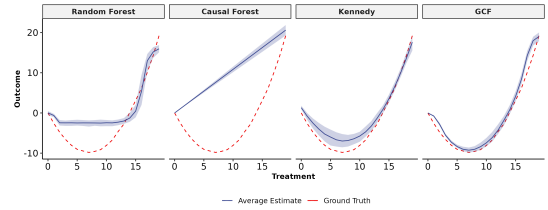


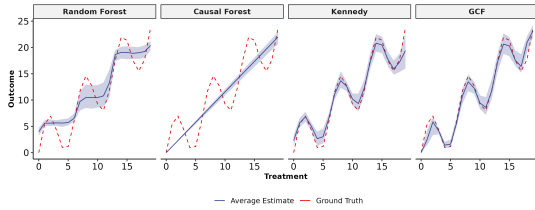
Figure 8: The estimated ADRF curve given by different models where the blue line is the estimation and red dash line is the ground truth on the dataset with DRF being poly and  $n = 1000, N = 100, p_X = 50, p_U = 5, p_Z = 5$

**Table 4: Simulation Results on Different data sets**

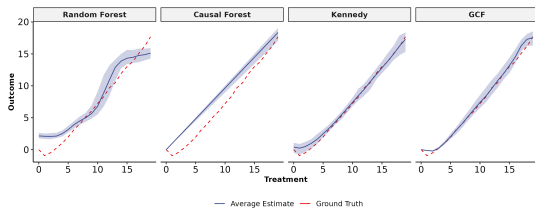
<i>Setup: 1k,100,100,10,10</i>						
Methods	<i>Polynomial</i>		<i>Sinusoidal</i>		<i>Exponential</i>	
	PEHE	RMSE	PEHE	RMSE	PEHE	RMSE
RF	8.08(0.4)	7(0.4)	4.89(0.4)	3.74(0.2)	4.28(0.4)	3.3(0.2)
CF	13.58(0.4)	12.04(0.4)	5.13(0.3)	3.96(0.2)	4.27(0.3)	3.25(0.2)
Kennedy	4.36(0.4)	3.27(0.3)	4.16(0.4)	2.75(0.2)	3.9(0.4)	2.56(0.2)
<b>GCF</b>	<b>4.3(0.3)</b>	<b>3.01(0.2)</b>	<b>4.19(0.4)</b>	<b>2.86(0.2)</b>	<b>3.91(0.4)</b>	<b>2.53(0.2)</b>

<i>Setup: 1k,100,50,5,5</i>						
Methods	<i>Polynomial</i>		<i>Sinusoidal</i>		<i>Exponential</i>	
	PEHE	RMSE	PEHE	RMSE	PEHE	RMSE
RF	5.63(0.4)	4.61(0.3)	4.27(0.4)	3.21(0.2)	3.57(0.4)	2.62(0.2)
CF	14.09(0.4)	12.58(0.4)	5.15(0.4)	3.96(0.2)	4.34(0.3)	3.37(0.2)
Kennedy	4.37(0.5)	3.36(0.5)	4.14(0.5)	2.78(0.3)	3.86(0.4)	2.54(0.2)
<b>GCF</b>	<b>4.14(0.3)</b>	<b>2.88(0.2)</b>	<b>4.05(0.4)</b>	<b>2.7(0.3)</b>	<b>3.85(0.4)</b>	<b>2.48(0.2)</b>



**Figure 9: The estimated ADRF curve given by different models where the blue line is the estimation and red dash line is the ground truth on the dataset with DRF being sinus and  $n = 1000, N = 100, p_X = 50, p_U = 5, p_Z = 5$**



**Figure 10: The estimated ADRF curve given by different models where the blue line is the estimation and red dash line is the ground truth on the dataset with DRF being exp and  $n = 1000, N = 100, p_X = 50, p_U = 5, p_Z = 5$**

## 8.5 Hyper-parameters

Both RF and CF use *num.trees* equals to 500, *min.node.size* to 50. For Kennedy [17], we use the code of function *cts.eff* from R package *npcausal* [5]. SuperLearner library is set to *SL.ranger* and *SL.glm*. We made small tweaks to *SL.ranger* to make share same hyperparameters with RF and CF for comparability.

## 8.6 Spark Implementation

Apache Spark [21] has the power of large-scale data processing and provides APIs of any machine learning algorithms. Consequently, we build our proposed algorithm on Spark to do parallel computing and distributed model training that leverage the resources of multiple machines simultaneously.

The workflow of Spark with GCF is shown in Figure 11, which include integrated data and distributed computation. More specifically, with the parallel structure of spark, the tree-growing process runs and the process of GCF is depicted in Figure 12, which is significantly different from that in CF [1] by distributing tasks for computations.

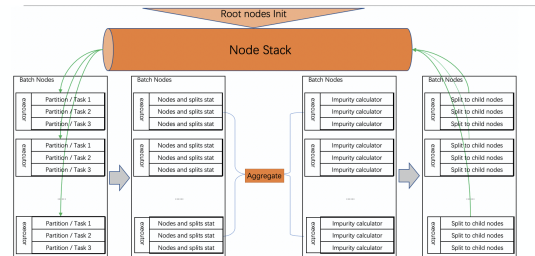


**Figure 11: Parallel architecture of GCF Spark Implementation. Data are partitioned at the nodes level and distributed across executors to achieve high performance**

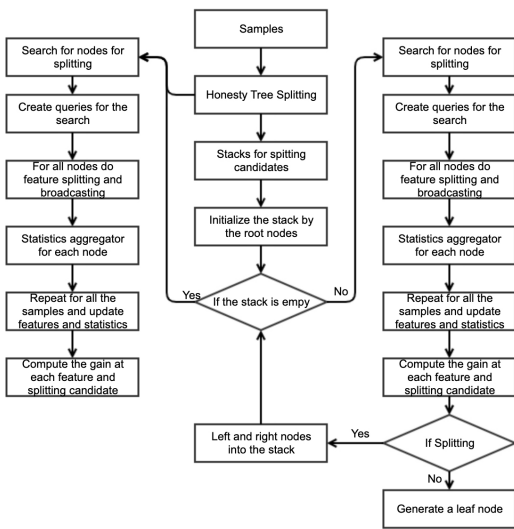


Figure 12: GCF algorithm workflow